Dalton Transactions

ROYAL SOCIETY OF CHEMISTRY

PAPER

View Article Online
View Journal | View Issue

Cite this: *Dalton Trans.*, 2024, **53**, 13384

Synergistic effects of the substrate–ligand interaction in metal–organic complexes on the de-electronation kinetics of a vitamin C fuel cell†

Muskan Parmar,‡[a] Sanchayita Mukhopadhyay,‡[a] Ritwik Mondal,‡[a] Bhojkumar Nayak,[a] Neethu Christudas Dargily,[a] Harish Makri Nimbegondi Kotresh,[b] Chathakudath Prabhakaran Vinod[c] and Musthafa Ottakam Thotiyl*[a]

The rising demand for portable energy conversion devices has spurred the advancement of direct liquid fuel cells (DLFCs) employing fuels such as alcohol, ammonia, hydrazine, and vitamin C. In these devices, various precious metal platforms have been explored to increase the de-electronation kinetics and reduce catalyst poisoning, but with substantial cost implications. We demonstrate the crucial role of ligands in non-precious organometallic complexes in influencing the de-electronation kinetics of fuel molecules through a unique substrate–ligand synergistic interaction. This unique chemistry imparts electron deficiency at the catalytic metal center while simultaneously populating the ligand with an extensive proton charge assembly. This distinct substrate–ligand interaction enhances the DLFC performance by coulombically dragging the substrate with a distinct amplification in its de-electronation kinetics. By integrating this approach with a ferricyanide/ferrocyanide half-cell reaction, a precious metal-free vitamin C fuel cell is developed, which is capable of generating an open circuit voltage of ~950 mV, a peak power density of ~97 mW cm^{-2} at a peak current density of ~215 mA cm^{-2} with the performance metrics nearly 1.7 times higher than a precious metal based DLFC. This highlights the potential of the substrate–ligand synergy in the design of efficient molecular catalysts for energy conversion applications.

Received 9th May 2024,
Accepted 15th July 2024

DOI: 10.1039/d4dt01370k

rsc.li/dalton

Introduction

The pursuit of electrochemical energy storage and conversion devices is driven by the growing need for electronic devices, medical equipment, electric cars, and resilient power systems.[1–5] The demand for long-lasting technologies has spurred increased research in the energy field, creating a constant challenge.[6–10] To address these needs, there have been explorations into the development of batteries, supercapacitors, fuel cells, and electrolyzers as electrochemical energy storage and conversion devices.[11–16] These devices heavily rely on their electrode components, particularly the anodes and cathodes where electrocatalysis occurs, shaping the overall device performance.[17–19] One interesting approach involves utilizing fuel cells (DLFCs), which include direct alcohol fuel cells, direct hydrazine fuel cells, and biomass-based fuel cells.[19–22] DLFCs function by tapping into the stored energy in fuels like alcohols, amines, and other compounds derived from biomass while taking oxygen from the air around them. However, DLFCs present challenges, such as safety issues with liquid fuels because of their toxicity and potential catalyst poisoning.[22,23] Nevertheless, DLFCs that use ascorbic acid (AA) as a fuel in the cell are particularly appealing due to their natural abundance in sources like citrus fruits. Making vitamin C through processes involving glucose fermentation and biowaste allows for this compound's access, transport, and storage.[21,24,25] To enhance the efficiency of vitamin C fuel cells, various precious metal electrocatalysts have been explored to boost the oxidation of vitamin C while being more resistant to poisoning.[26–29]

In these contexts, molecular electrocatalysts featuring the N_4-macrocyclic framework, like metal phthalocyanines, have received attention as viable non-precious electrocatalysts for various electrochemical processes due to their tunable opto-electronic properties and exceptional chemical and thermal durability.[30–32] These molecular electrocatalysts show fast

[a]*Department of Chemistry and Centre for Energy Science, Indian Institute of Science Education and Research, Pune, Dr Homi Bhabha Road, Pune 411008, India. E-mail: musthafa@iiserpune.ac.in*
[b]*Department of Chemistry, Acharya Institute of Technology, Soldevanahalli, Bangalore 560701, India*
[c]*Catalysis and Inorganic Division, CSIR-NCL, Pune 411008, India*

†Electronic supplementary information (ESI) available: Tables S1–S3, graphics (Fig. S1–S21) and calculations. See DOI: https://doi.org/10.1039/d4dt01370k

‡These authors contributed equally.

redox processes as well as low reorganizational energies, making them efficient redox mediators in electron transfer reactions.[33–36] In contrast to previous investigations concentrating on MN_4 electrocatalysts and the nature of the central metal ion,[37–39] our current investigation aims to examine the role of ligands within the N_4 macrocyclic framework for boosting the performance of vitamin C DLFCs. Our study specifically delves into how the ligands around the same catalytic metal center can enhance the electrochemical processes during ascorbic acid oxidation *via* a ligand-assisted extensive proton charge assembly and electron density alteration. Additionally, in our effort to create a precious metal-free vitamin C fuel cell, we have explored the substitution of the cathodic half-cell, traditionally employing the oxygen reduction reaction (ORR), with an outer sphere redox species capable of efficiently transporting electrons, particularly on carbon-based electrodes. This judicious coupling has eventually led to a precious metal-free vitamin C fuel cell with an open circuit voltage of nearly 950 mV and a peak power density of ~97 mW cm^{-2} at a peak current density of ~215 mA cm^{-2}.

Results and discussion

To ascertain the substrate–ligand synergistic interaction in vitamin C oxidative electrocatalysis, unsubstituted copper phthalocyanine (CuPc) and the amino-substituted copper phthalocyanine (TACuPc) molecules (Fig. 1a) were synthesized according to the reported procedures (please refer to the Experimental section in the ESI†). Cu was chosen as the central metal because of its well-reported capability of oxidizing small organic molecules and its high chelation affinity towards the ascorbate anion.[40–44] Following their synthesis, both molecules were thoroughly characterized using various spectrochemical techniques.[45–49] Initially, Fourier transform infrared (FT-IR) spectroscopy was carried out as shown in Fig. 1b. FT-IR analysis of CuPc and TACuPc revealed characteristic peaks at 550–950 cm^{-1}, ~1110 cm^{-1}, 1290–1390 cm^{-1}, and ~2880–3200 cm^{-1} corresponding to phthalocyanine skeletal vibrations, C–N bending, C–N stretching and C–H stretching vibration, respectively (Fig. 1b). Additional peaks at 3200 to 3500 cm^{-1} (N–H stretching) and 1619 cm^{-1} (N–H bending) in TACuPc confirmed the incorporation of the primary amine functionality onto the phthalocyanine ring (Fig. 1b). Furthermore, matrix assisted laser desorption ionization-time of flight (MALDI-TOF) mass spectrometry confirmed the expected molecular ion peaks for CuPc and TACuPc at m/z values of ~576 and ~636 (Fig. S1†). The UV-visible spectra exhibited two bands at around 350 nm and 700 nm corresponding to the B-band and Q-band of phthalocyanine molecules, respectively (Fig. 1c). The Q band was found to be red-shifted for TACuPc compared to CuPc, indicating enhanced delocalization because of the presence of the NH_2 functionality attached to the macrocyclic ring in the TACuPc molecule. Raman spectra (Fig. 1d) of the molecules show macrocyclic stretching at around ~700 cm^{-1}, and C–H bending and C–H in-plane deformation at ~1130 cm^{-1} and ~1210 cm^{-1}, respectively. Pyrrole in-plane stretching bands are observed at ~1350 cm^{-1}. The band at around ~1533 cm^{-1} is consistent in both molecules, representing the macrocyclic in-plane stretching. NMR spectroscopy analysis was performed with the corresponding nickel phthalocyanines (NiPc) and tetra amino nickel phthalocyanine (TANiPc) since the central Cu metal in CuPc and TACuPc is paramagnetic. The NMR spectra of NiPc show two aromatic ring protons designated as H_a and H_b, as shown by the orange trace in Fig. 1e. TANiPc revealed four distinct peaks for aromatic ring protons at ~8.8 ppm, ~8.4 ppm, and ~7.4 ppm, marked as H_c, H_f, and H_d. The peak at ~6.4 ppm indicates the presence of the amino group, Fig. 1e (blue trace). Scanning electron microscopy was performed to verify the morphologies of the synthesized CuPc and TACuPc molecules. CuPc exhibits a rodlike morphology, whereas the TACuPc shows an aggregated morphology, which is in line with previous literature (Fig. 1f).[50,51] The elemental mapping (EDX images) is shown in Fig. 1g, which confirms the uniform distribution of Cu, N, and C throughout. Overall, these characterizations substantiate the successful formation of both molecules.

Anodic half-cell chemistry

To electrochemically characterize both molecules, cyclic voltammetry (Fig. S2a†) was performed in a pH 7 electrolyte in the absence of ascorbic acid. Differential pulse voltammetry was further carried out in the same blank electrolyte with both molecules (Fig. S2b†). The results show the redox transitions of the central metal ion, which is much more prominent and negatively shifted in TACuPc compared to CuPc. To understand the role of a substrate–ligand synergistic interaction in assisting the anodic half-cell reaction, the activity of CuPc and TACuPc was probed towards vitamin C (ascorbic acid) oxidation. Cyclic voltammetry was performed in an argon-saturated 0.1 M phosphate buffer solution (pH ~ 7) at a scan rate of 10 mV s^{-1}, and after the addition of ascorbic acid, the pH of the solution was shifted towards the acidic side (pH ~ 2). This happened because ascorbic acid was dissociated into the ascorbate anion and protons, which decreased the pH. It was observed that tetra amino copper phthalocyanine (TACuPc) exhibited a notably lower onset potential and a higher current density than the unsubstituted copper phthalocyanine (CuPc) molecule (Fig. 2a). It should be noted that the redox transitions of the central metal ion are commensurate to the onset potential observed for ascorbic acid oxidation (Fig. S2† and Fig. 2a). On comparing with the noble metal electrocatalyst platinum (Pt), the molecular electrocatalysts were found to be more active towards vitamin C oxidation (Fig. 2a). The chronopotentiometry attests to the long-term stability and durability of the electrocatalyst towards vitamin C oxidation (Fig. 2b). Similar to the onset potential, TACuPc required less overpotential compared to CuPc to attain a specific current density. This activity is found to be better than that of Pt-based electrocatalysts (Fig. 2a and b). The lower activity on Pt may be explained

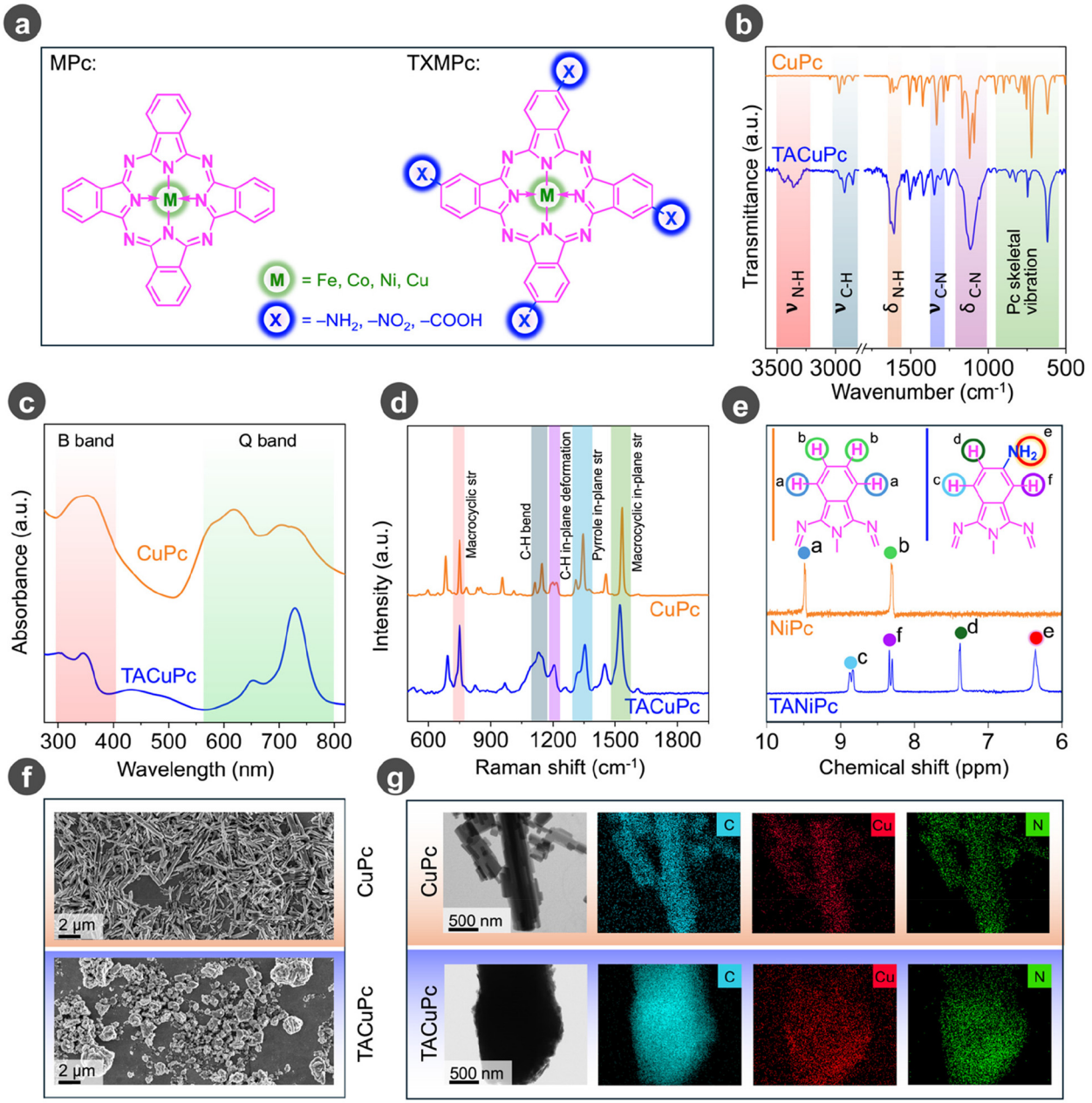

Fig. 1 (a) Chemical structure, (b) FT-IR spectra, (c) UV-visible spectra, and (d) Raman spectra of CuPc and TACuPc molecules. (e) NMR spectra of NiPc and TANiPc molecules. (f–g) SEM, TEM and elemental mapping (Cu, C, N) of CuPc and TACuPc molecules.

by its susceptibility to poisoning by ascorbic acid or its oxidized products.[52,53] In addition, we have investigated the product formed from the electrolyte. Dehydroascorbic acid (DHA) was present in the post-reaction electrolyte after the reaction (Fig. S3†).[54] To further investigate the kinetics of vitamin C oxidation, the Tafel slope was determined, and TACuPc (~113 mV dec^{-1}) was found to have a lower Tafel slope than CuPc (~162 mV dec^{-1}), suggesting facile kinetics during a vitamin C reaction on the TACuPc molecule (Fig. 2c). The electrochemical impedance spectroscopy (EIS) analysis of both the molecules carried out at an open circuit voltage (OCV) indicates a lower charge transfer resistance (R_{ct}) for TACuPc compared to CuPc, signifying its superior activity over CuPc (Fig. 2d and Table S1†). In the equivalent circuit used for fitting a series RC circuit combination is utilized (inset of Fig. 2d). The pairing of Q_1 and R_1 in parallel within the initial RC circuit (starting from the left) symbolizes the geometrical capacitance of the catalyst and the resistance of the film layer, respectively. In tandem with this initial RC parallel setup, the subsequent RC circuit, comprising a constant phase element Q_2, a resistance R_{ct}, and a Warburg impedance Z_W, delineates the interfacial capacitance, charge-transfer resistance, and the

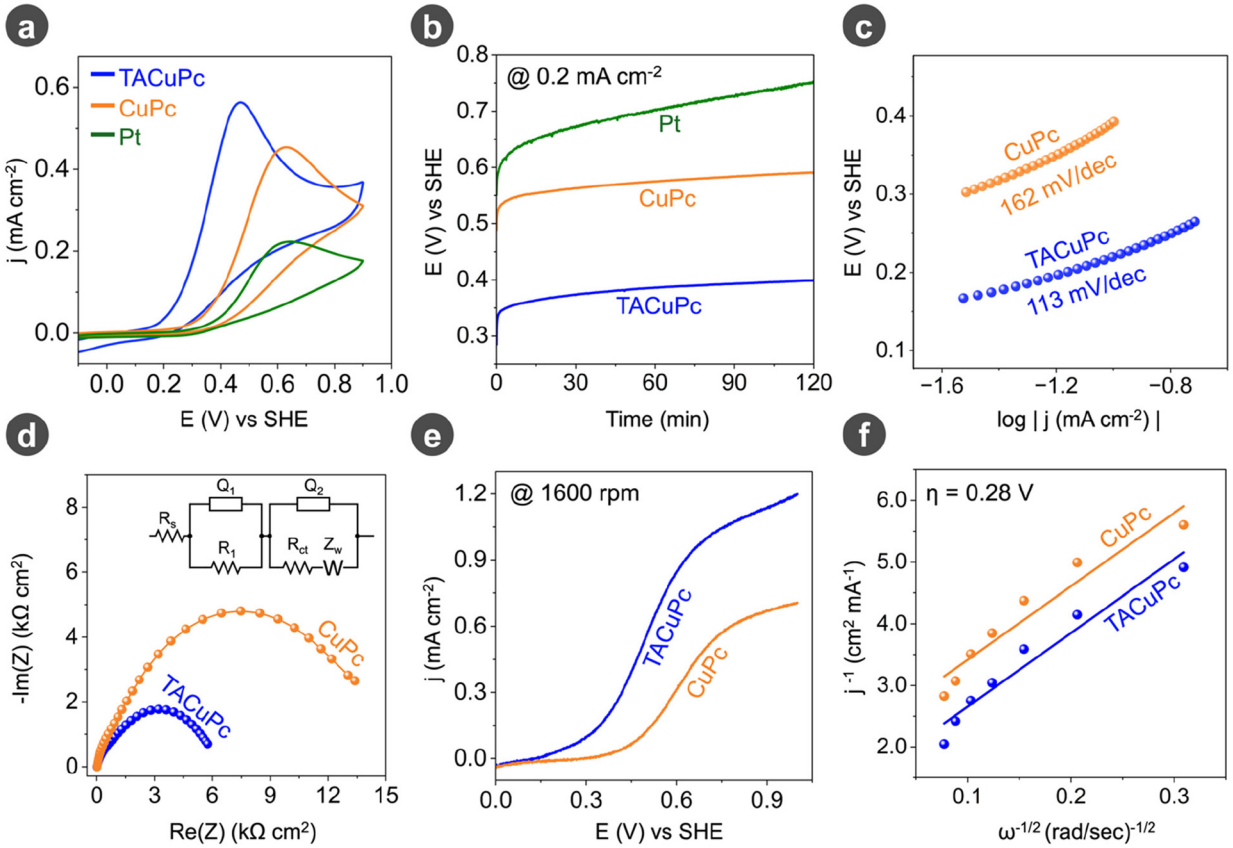

Fig. 2 (a) Cyclic voltammograms of ascorbic acid oxidation (in phosphate buffer at pH 7) at a scan rate of 10 mV s^{-1} and (b) chronopotentiometric traces at a current density of 0.2 mA cm^{-2} with CuPc, TACuPc and Pt electrocatalysts. (c) Tafel plots and (d) electrochemical impedance spectra (EIS) collected at an open circuit voltage (OCV) in the frequency range of 100 kHz to 1 mHz with a 10 mV AC amplitude (peak-to-peak) for CuPc and TACuPc molecules. Inset of Fig. 2d shows the equivalent circuit used for fitting. (e) Rotating disk electrode measurements for ascorbic acid oxidation in phosphate buffer (pH 7) and (f) the corresponding Koutecky–Levich (K–L) plot at an overpotential of 0.28 V with respect to the onset potential for CuPc and TACuPc molecules.

mass transport aspect of active species to and from the electrode surface, respectively. To gain a better insight, the scan rate dependence study of ascorbic acid oxidation for both the catalysts was performed by varying the scan rate at a constant vitamin C concentration, and the logarithmic plot of the peak current density *versus* the scan rate exhibited a slope of ~0.5 (Fig. S4†), which indicates a diffusion-controlled process at sufficiently positive potentials. Furthermore, the current density was found to increase linearly with a gradual increment of vitamin C concentration in the electrolyte (Fig. S5†). To understand how the ligand influences the kinetics and mechanism of this reaction, we employed a hydrodynamic technique that involved the use of rotating disc electrodes (RDE) at various rotation rates. TACuPc showed a superior onset potential and current density to CuPc at any rotation rate (Fig. 2e and Fig. S6†). A Koutecky–Levich (K–L) plot obtained from RDE analysis (Fig. S7†) demonstrated that the number of electrons participating in the reaction was ~2 for both the molecules (Fig. 2f). All the above results suggest that the fundamental reaction mechanism governing the oxidation of ascorbic acid obtained from RDE analysis (Fig. S7†) remained consistent for both the molecules; however, their kinetics were influenced by the nature of the ligand.

In order to find the underlying reason behind the enhanced activity of TACuPc compared to the unsubstituted CuPc, we analyzed the molecules by X-ray Photoelectron Spectroscopy (XPS). The N 1s spectra of unsubstituted CuPc can be deconvoluted into two peaks, with the B.E. order N_1 (Cu–N) < N_2 (–C═N), in its pristine state (Fig. 3a, bottom panel), whereas the N 1s regime in the XPS spectra of TACuPc consists of three distinct peaks with the binding energy (B.E.) order: N_1 (Cu–N) < N_2 (–C═N) < N_3 (–C–NH_2) (Fig. 3b. bottom panel).[55–57] Upon treatment of both the molecules with the electrolyte solution containing ascorbic acid, we observed an upshift (top panel of Fig. 3a and b) in the binding energies of the N 1s spectra, as compared to their pristine states. These upshifts in binding energy can be explained by the proton charge assembly over the nitrogen moieties by its chemical interaction with the ascorbic acid substrate.[58–60] Since there is a higher number of N centers in TACuPc, the proton charge assembly over this molecule should be comparatively extensive, and hence this

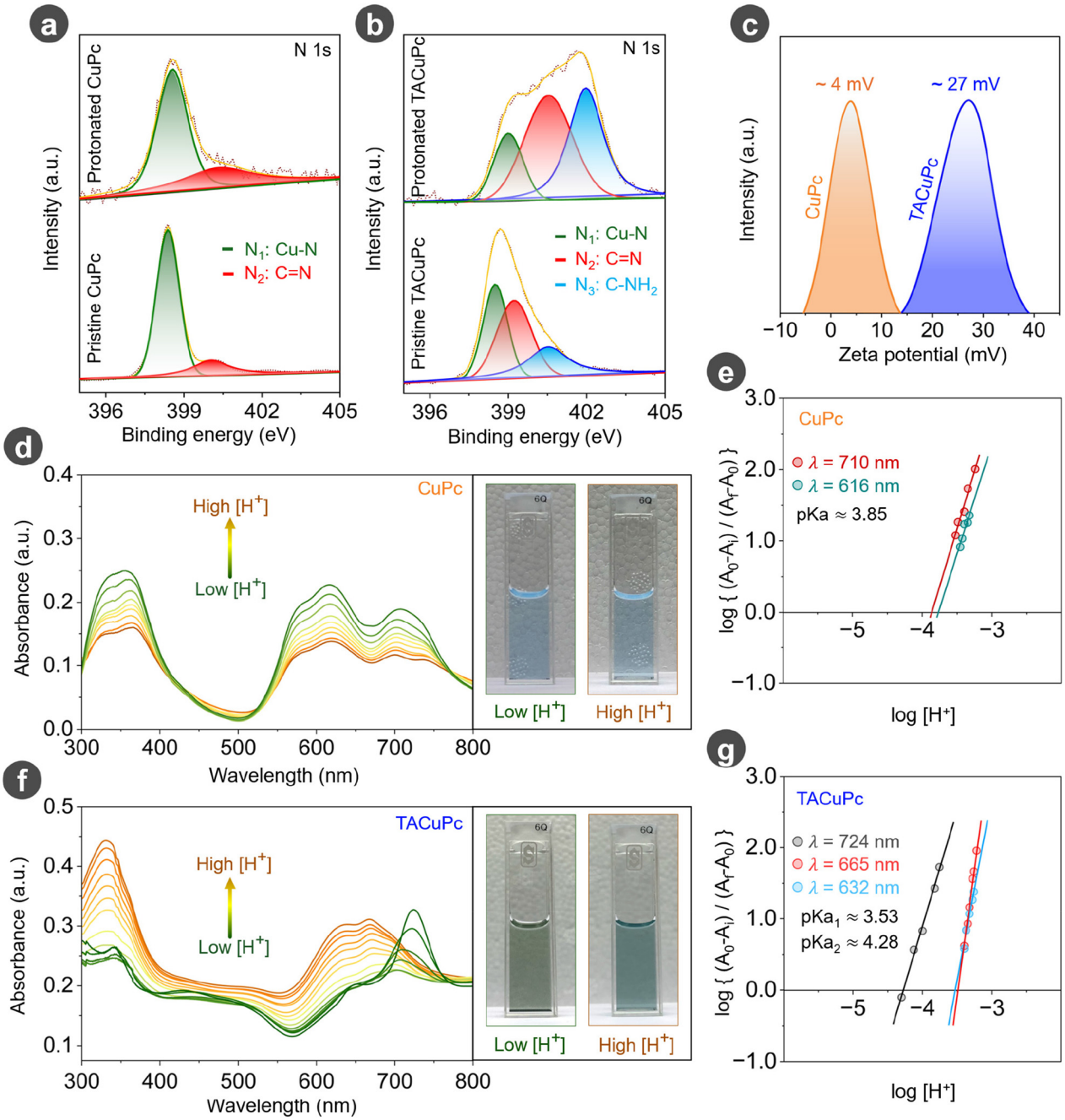

Fig. 3 (a and b) N1s XPS spectra of pristine and protonated (after treating with ascorbic acid) CuPc and TACuPc. (c) Zeta potential measurements of CuPc and TACuPc molecules in the electrolytic medium. (d) UV-visible spectra of CuPc during the continuous addition of protons and (e) the corresponding Hill plot at different wavelengths. (f) UV-visible spectra of TACuPc during the continuous addition of protons and (g) the corresponding Hill plot at different wavelengths. The insets of Fig. 3d and f show photographs of the molecular catalyst solution at low and high concentrations of protons.

molecule should exhibit a large BE shift compared to unsubstituted CuPc. This is indeed found to be true as detailed in Fig. 3a, b and Fig. S8 and Table S2.† In order to understand how this proton charge assembly tunes the electron density at the catalytic Cu centre, Cu 2p XPS spectra were analyzed (Fig. S9a and b†). It can be noted that the Cu $2p_{3/2}$ peak of protonated TACuPc and CuPc has upshifted to higher binding energies compared to their pristine states (Fig. S9a and b.†). This upshift is found to be much more pronounced in TACuPc due to its extensive proton charge assembly, which decreases the electron donation from N towards Cu, making the catalytic Cu centre more electron deficient. Taken together, the N 1s and Cu 2p spectra imply that TACuPc has extensive proton charge assembly and its catalytic Cu centre experiences notice-

able oxidative activation. To substantiate our claim, the electrical double layer (EDL) of both the catalysts in the electrolytic medium containing ascorbic acid was measured. TACuPc exhibited a higher EDL than CuPc (Fig. S10a†). This indicates a higher surface charge for TACuPc than CuPc. To check the nature of the surface charge, a negatively charged redox probe (ferricyanide) was introduced into the system (Fig. S10b†). The current was found to be higher in the case of TACuPc than in CuPc, indicating the surface of TACuPc to be more positive than CuPc. Similarly, on introducing a positively charged redox species (ruthenium hexamine chloride) into the medium, a reverse trend was observed (Fig. S10c†). For the magnitude of surface charge, zeta potential measurements were performed, and the results confirmed a substantially positive surface charge for TACuPc compared to CuPc (Fig. 3c). We further confirmed this by obtaining the UV-visible spectra of both the molecules before and after the introduction of ascorbic acid (Fig. S11†). The addition of ascorbic acid to the medium resulted in a pronounced blue shift of the Q-band towards a lower wavelength, especially for the TACuPc molecule compared to the unsubstituted CuPc molecule (Fig. S11†). To further verify the extent of protonation of TACuPc and CuPc, we have determined the pK_a of the nitrogen atoms in the CuPc and TACuPc molecules using UV-visible titration and the Hill plot. For CuPc, the intensity of the Q band at 616 and 710 nm decreased during continuous acid addition (Fig. 3d). From the Hill plot, the pK_a was around 3.77 (616 nm) and 3.85 (710 nm), Fig. 3e. In the case of TACuPc, the characteristic Q band in the range 550–780 nm is blue-shifted with intensity variations during acid addition (Fig. 3f). From the Hill plot, the pK_a was nearly 4.28 (724 nm) and 3.53 (665 nm), Fig. 3g. Ascorbic acid (AA) has two pK_a values of 4.1 and 11.6.[61,62] According to acid–base chemistry principles, a lower pK_a value corresponds to a stronger acid.[63] Therefore, ascorbic acid should protonate the TACuPc extensively. This claim is further supported by the optical images of the solution before and after the addition of acid. For TACuPc, a visible color change was observed during acid addition but no such visible color change was present in the case of CuPc. Therefore, these analyses suggest that a substrate–ligand synergy exists prominently in TACuPc compared to CuPc. All this corroborates the fact that the surface charge is indeed more positive in TACuPc, which is facilitated by the substrate-assisted proton charge assembly over the ligand. Thus, TACuPc, having a more positive surface charge, should exert a higher coulombic attraction on the negatively charged ascorbate anion than CuPc, thereby generating an additional electrostatic current contribution over the diffusion current. The de-electronation of vitamin C should be further facilitated over the TACuPc catalyst by the oxidative activation of its catalytic Cu center, as demonstrated in Fig. S9.†[64–66] It is established that the oxidized form of copper can chelate more efficiently with the ascorbate ion.[67,68] In order to assess the same, *ex situ* Raman spectra of the molecular catalysts exposed to ascorbic acid at the open circuit potential (OCP) were obtained (for details, refer to the Experimental section). The normalized spectrum, as shown in Fig. S12a,† clearly depicts a noticeable alteration to the key features of TACuPc, but little to CuPc. The ratios of intensities of the four prominent bands marked 1–4 in the pre/post characterization spectrum (Fig. S12b†) further attest to the same. Out of these, peaks in the regime of 650–770 cm^{-1} are known to have contributions from metal to ligand bonds.[69–71] Therefore, the intensity rise nearing almost double in TACuPc can be attributed to the modifications in the metal to ligand bonds in the presence of ascorbic acid. Conversely, in CuPc such interactions are negligible as only little modifications are observed in their Raman spectra before and after ascorbic acid treatments. This is supported by the enhanced oxidative activation of the Cu metal centre in TACuPc as shown in Fig. S9†, leading to better chelation of the ascorbate ion with TACuPc as compared to CuPc (Scheme S1†). This, in turn, facilitates a more facile oxidation of ascorbic acid in the case of TACuPc as compared to CuPc. These combined effects of oxidative activation of the central metal ion and the stronger electrostatic current due to larger interfacial accumulation of proton charge assembly explain the better activity of TACuPc over CuPc towards vitamin C oxidation. It should be noted that this oxidative activation of the central metal ion and the interfacial proton charge assembly over the ligand are aided by the chemical interaction of ascorbic acid (which is the substrate) with the catalyst molecules, as demonstrated by a series of experiments in Fig. 3. Therefore, this demonstration presents a unique example of a substrate–ligand chemistry assisted boosting of substrate electrocatalysis.

Cathodic half-cell chemistry

In order to elucidate a Pt-free vitamin C fuel cell configuration, we replaced a conventional oxygen reduction half-cell by ferricyanide redox chemistry. This reaction has recently been used as the cathodic half-cell chemistry in a wide range of devices due to their fast electrochemical kinetics even on carbon-based electrodes.[72,73] To elucidate the potential of ferricyanide redox as an electron acceptor, experiments were performed on carbon-based electrodes. The cyclic voltammetry in Fig. S13a† exhibits a peak separation of nearly 69 mV, closely aligned with the expected value of 59 mV for a rapid and reversible one-electron transfer reaction. Additionally, the logarithm of the peak current density *versus* the logarithm of the scan rate displayed a slope of around 0.5, suggesting a diffusion-controlled process (Fig. S13b†). From RDE and the K–L plot the number of electrons involved in the reaction was found to be ~1 (Fig. S14a and b†). Furthermore, the plot of the overpotential *versus* the logarithm of kinetic current, as depicted in Fig. S14c,† provided the rate constant for the ferricyanide/ferrocyanide redox couple, which was 2.9×10^{-2} cm s^{-1}. These values strongly suggested the occurrence of a rapid redox reaction of a ferricyanide/ferrocyanide outer sphere redox couple even on carbon electrodes. Based on the aforementioned results, ferricyanide was chosen as the electron acceptor on the

carbon-based electrode for the proposed precious metal-free vitamin C fuel cell.

Fuel cell performance

In order to assess the fuel cell performance, we first performed the fuel cell study in neutral media (pH = 7). From the single-electrode potential analysis in neutral media (Fig. 4a), we have an overall voltage output of nearly 0.6 V. The single electrode potentials observed for vitamin C on TACuPc (cyan trace) and ferricyanide (red trace) on a carbon-based electrode exemplify that vitamin C acts as an electron donor (Fig. 4a). In contrast, ferricyanide fulfills the role of an electron acceptor in the proposed configuration. Hence, the reduction of ferricyanide serves as the cathodic reaction (eqn (1)) and the oxidation of vitamin C as the anodic reaction (eqn (2)). The complete cell reaction (eqn (3)) involves the oxidation of vitamin C (ascorbic

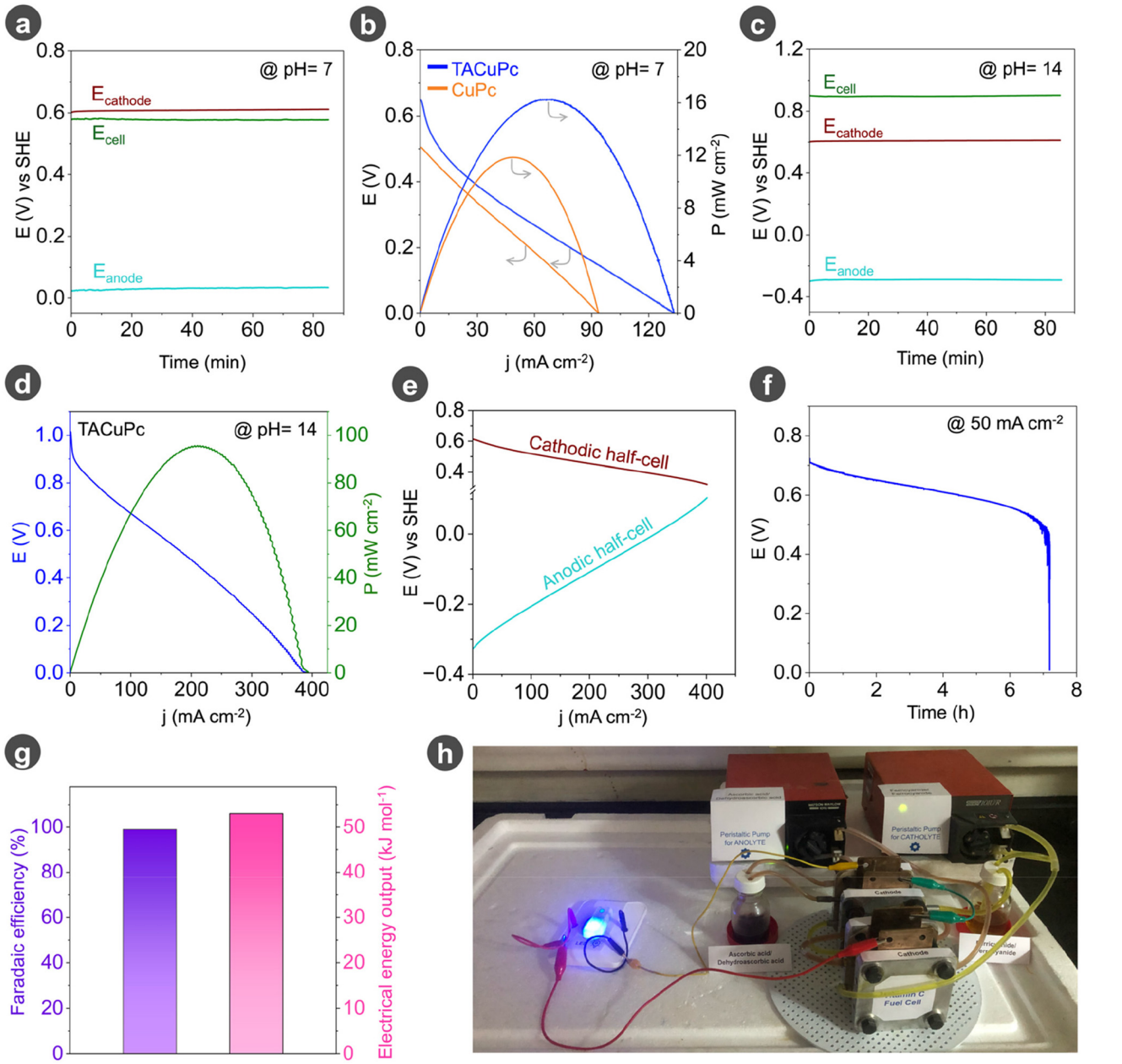

Fig. 4 (a) Single electrode potential and open circuit voltage plot for the TACuPc modified vitamin C fuel cell at pH 7 electrolytes. (b) Polarization curves for both CuPc and TACuPc modified vitamin C fuel cells at pH 7 electrolytes. (c) Single electrode potential and open circuit voltage plot for the TACuPc modified vitamin C fuel cell at pH 14 electrolytes. (d) Polarization curves for the TACuPc modified platinum-free vitamin C fuel cell in pH 14 electrolytes. (e) Half-cell polarization (anodic and cathodic) for the TACuPc modified vitamin C fuel cell. (f) Chronopotentiometry at a constant current density of 50 mA cm^{-2}. (g) Energy output and faradaic efficiency for the vitamin C fuel cell. (h) Photograph of the platinum-free vitamin C fuel cell powering a 1.5 V commercial LED.

acid) to dehydroascorbic acid and the reduction of ferricyanide to ferrocyanide, enabling an electron flow through the external circuit. The fuel cell performance was verified with both the molecules CuPc and TACuPc as anodic electrocatalysts and TACuPc has the upper hand in the fuel cell performance (Fig. 4b). From polarization analysis with TACuPc as the anodic electrocatalyst, a peak power density of 16 mW cm^{-2} at a peak current density of 70 mA cm^{-2} was achieved (Fig. 4b). The current and power normalized to the actual loading of the molecular catalysts further demonstrated an amplified performance metrics in favour of the TACuPc molecular catalyst (Table S3†). In order to enhance the overall potential window and electrical output, we further carried out the fuel cell study in an alkaline medium, where a higher open circuit voltage was achieved in alkaline media as compared to the neutral media (Fig. 4c). The performance metrics of the above-mentioned vitamin C fuel cell was measured using polarization curves. In alkaline media, the platinum-free vitamin C fuel cell is shown to have an open circuit voltage (OCV) of approximately 0.95 V and a peak power density of nearly 97 mW cm^{-2} at a peak current density of 215 mA cm^{-2} (Fig. 4d).

Cathodic reaction:

$$2[Fe(CN)_6]^{3-} + 2e^- \rightleftharpoons 2[Fe(CN)_6]^{4-} \quad (1)$$

Anodic reaction:

$$C_6H_8O_6 \rightleftharpoons C_6H_6O_6 + 2H^+ + 2e^- \quad (2)$$

Overall reaction:

$$2[Fe(CN)_6]^{3-} + C_6H_8O_6 \rightleftharpoons C_6H_6O_6 + 2[Fe(CN)_6]^{4-} + 2H^+ \quad (3)$$

The performance of the TACuPc catalyzed vitamin C fuel cell is 1.7 times superior in terms of power density to that of Pt-based fuel cells (Fig. S15†). The study of individual half-cell polarization (Fig. 4e) of the TACuPc catalyzed vitamin C fuel cell provides evidence that the anodic half-cell reaction is limiting the overall performance and efficiency of the entire system. This performance deficit can be attributed to the lower electrode kinetics of vitamin C oxidation compared to that of ferricyanide. The long-term study suggests that the fuel cell, equipped with a vitamin C-$[Fe(CN)_6]^{3-}/[Fe(CN)_6]^{4-}$ redox couple, can operate for several hours (Fig. 4f), suggesting that it exhibits an impressive level of stability at both interfaces. To further confirm the mechanism of the cell, the charge passed and the consumption of ferricyanide in the catholyte were estimated. For this, we have conducted UV-visible analysis at various time intervals during the chronopotentiometry experiments (Fig. S16a†). The charge balance shows almost a linear correlation between the charge passed and the ferricyanide consumed (Fig. S16b†). *Ex situ* UV-visible analysis was used to determine the ferricyanide consumption in the catholyte and its concentration was estimated based on the calibration plot provided in Fig. S17.† As shown in Fig. 4g, a lab-scale prototype can deliver nearly 53 kJ $mol_{Ferricyanide}^{-1}$ of electrical energy output with nearly 99.9% of faradaic efficiency (refer to Calculation S1 in the ESI†). In order to understand the self-discharge rate of this Pt-free vitamin C fuel cell, we have carried out open circuit potential measurements for 50 hours (Fig. S18a†) in the fuel cell mode. To determine the exact concentration of vitamin C before and after self-discharge measurements, we have carried out UV-vis spectroscopy analysis of the electrolyte before and after 50 hours of self-discharge (Fig. S18b†). A slight change in the concentration of vitamin C from 1 M to 0.905 M occurred in 50 hours, which corresponds to approximately 70 mV of open circuit potential change (Fig. S18c†). A self-discharge rate of 1.4 mV h^{-1} is observed for this vitamin C fuel cell, with a concentration change of 1.9 mM per hour (Fig. S18d†, refer to Calculation S2 in the ESI†). The concentration of vitamin C in the electrolyte was measured using a calibration plot obtained from UV-vis spectroscopy at various known concentrations of vitamin C, (Fig. S19†). We demonstrate that this laboratory-scale Pt-free vitamin C fuel cell can power an LED and a motor, suggesting its usefulness (Fig. 4h and ESI Video S1†) in portable electronic devices. In summary, by utilizing the substrate assisted proton charge assembly over TACuPc and its subsequent oxidative activation, we have designed a precious metal-free vitamin C fuel cell, with performance metrics nearly 1.7 times higher than Pt based vitamin C fuel cells.

Conclusions

The development of efficient molecular electrocatalysts is crucial for enhancing the performance of energy conversion devices. By exploring a peculiar substrate–ligand synergistic interaction, we could influence the electron density at the catalytic central metal *via* an extensive proton charge assembly over the ligand. This has led to efficient de-electronation of vitamin C over a Cu-based metal phthalocyanine with an amplified mass transport, and on coupling this with a ferricyanide/ferrocyanide half-cell reaction on a carbon electrode, a precious metal-free vitamin C fuel cell could be designed. It should be noted that the oxidation of 1 mol of ascorbic acid releases 2 protons, which leads to a quick build-up of protons in the electrolyte. However, if a vitamin C fuel cell is designed where the cathodic reaction is a proton-consuming reaction such as the oxygen reduction reaction, this build-up of protons can be avoided. Therefore, in order to avoid this proton build-up, the counter-reaction has to be designed to consume the protons. Nevertheless, this investigation highlights the potential of a substrate–ligand synergistic interaction in designing effective molecular catalysts for sustainable energy conversion applications.

Author contributions

M. P. performed the experiments along with the assistance of S. M. and R. M. S. M. and R. M. analyzed all the data. B. N. recorded the video and helped in data plotting. N. C. D. helped

in data analysis. H. M. N. K. synthesized the molecules. C. P. V. helped with XPS analysis. M. O. T. conceived the idea and supervised the work.

Data availability

The data supporting this article have been included as part of the ESI.†

Conflicts of interest

The authors declare no conflict of interest.

Acknowledgements

M. O. T. is indebted to DST-SERB (CRG/2020/002549) and DST-WTI (DST/TMD-EWO/WTI/2K19/EWFH/2019/272) for financial support. M. P. acknowledges CSIR-UGC for a fellowship. S. M. and R. M. acknowledge IISER Pune, India, for financial assistance.

References

1 R. B. Jethwa, S. Mondal, B. Pant and S. A. Freunberger, *Angew. Chem., Int. Ed.*, 2024, e202316476.
2 R. Jommongkol, S. Deebansok, J. Deng, Y. Zhu, R. Bouchal and O. Fontaine, *Small*, 2024, **20**, 1–13.
3 F. Makhlooghiazad, L. Miguel Guerrero Mejía, G. Rollo-Walker, D. Kourati, M. Galceran, F. Chen, M. Deschamps, P. Howlett, L. A. O'Dell and M. Forsyth, *J. Am. Chem. Soc.*, 2024, **146**, 1992–2004.
4 S. Nikman, D. Zhao, V. Gonzalez-Perez, H. H. Hoster and S. F. L. Mertens, *Electrochim. Acta*, 2021, **386**, 138373.
5 M. Miroshnikov, K. Mahankali, N. K. Thangavel, S. Satapathy, L. M. R. Arava, P. M. Ajayan and G. John, *ChemSusChem*, 2020, **13**, 2186–2204.
6 L. Schulte, W. White, L. A. Renna and S. Ardo, *Joule*, 2021, **5**, 2380–2394.
7 D. Jaramillo, G. Alvarez, C. Díaz, S. Pérez, J. Muñoz Saldaña, L. Sierra, B. L. López, A. Moreno-Zuria, M. Mohamedi and R. Palacio, *Dalton Trans.*, 2023, **53**, 3143–3158.
8 A. Y. Ganin and M. D. Symes, *Curr. Opin. Electrochem.*, 2022, **34**, 101001.
9 J. Bisquert, *Phys. Rev. Appl.*, 2024, **10**, 1.
10 S. Deebansok, J. Deng, E. Le Calvez, Y. Zhu, O. Crosnier, T. Brousse and O. Fontaine, *Nat. Commun.*, 2024, **15**, 1133.
11 Y. K. Petit, E. Mourad, C. Prehal, C. Leypold, A. Windischbacher, D. Mijailovic, C. Slugovc, S. M. Borisov, E. Zojer, S. Brutti, O. Fontaine and S. A. Freunberger, *Nat. Chem.*, 2021, **13**, 465–471.
12 P. Prakash, B. Fall, J. Aguirre, L. A. Sonnenberg, P. R. Chinnam, S. Chereddy, D. A. Dikin, A. Venkatnathan, S. L. Wunder and M. J. Zdilla, *Nat. Mater.*, 2023, **22**, 627–635.
13 C. Prehal, S. Mondal, L. Lovicar and S. A. Freunberger, *ACS Energy Lett.*, 2022, **7**, 3112–3119.
14 J. Lei, Y. Zhang, Y. Yao, Y. Shi, K. L. Leung, J. Fan and Y.-C. Lu, *Nat. Energy*, 2023, **8**, 1355–1364.
15 P. A. Maughan, A. B. Naden, J. T. S. Irvine and A. R. Armstrong, *Batteries Supercaps*, 2023, **6**, 6–13.
16 R. Mondal, R. Thimmappa, B. Nayak, A. Dewan, M. C. Devendrachari, Q. Chen, Z. Wen and M. O. Thotiyl, *Energy Environ. Sci.*, 2023, **16**, 3860–3872.
17 Q. Zou, Z. Liang, W. Wang, D. Dong and Y. C. Lu, *Energy Environ. Sci.*, 2023, **16**, 6026–6034.
18 R. Sharma, H. Kumar, G. Kumar, S. Sharma, R. Aneja, A. K. Sharma, R. Kumar and P. Kumar, *Chem. Eng. J.*, 2023, **468**, 143706.
19 L. Durai and S. Badhulika, *Fuel*, 2023, **352**, 129058.
20 I. S. Pieta, R. G. Kadam, P. Pieta, D. Mrdenovic, R. Nowakowski, A. Bakandritsos, O. Tomanec, M. Petr, M. Otyepka, R. Kostecki, M. A. M. Khan, R. Zboril and M. B. Gawande, *Adv. Mater. Interfaces*, 2021, **8**, 2001822.
21 M. M. Hasan, *Electrochem*, 2023, **4**, 31–41.
22 J. Chang, G. Wang, C. Li, Y. He, Y. Zhu, W. Zhang, M. Sajid, A. Kara, M. Gu and Y. Yang, *Joule*, 2023, **7**, 587–602.
23 R. M. Altarawneh, *Energy Fuels*, 2021, **35**(15), 11594–11612.
24 C. Qiu, Q. Zhou, Y. Guo, J. Qin, D. Wang and Y. Song, *Nanomaterials*, 2023, **13**, 2669.
25 X. Yin, K. Chen, H. Cheng, X. Chen, S. Feng and Y. Song, *Antioxidants*, 2022, **11**, 1–20.
26 A. Keramati, K. Hendrix, D. Nguyen, F. Gonzales, K. Waters, A. Fry-Petit and J. L. Haan, *Int. J. Energy Res.*, 2021, **45**, 10821–10831.
27 M. Khairy and B. G. Mahmoud, *Electroanalysis*, 2016, **28**, 2606–2612.
28 P. Pal, S. Bhattacharjee, M. Paul Das, Y. B. Shim, B. Neppolian, B. J. Cho, P. Veluswamy and J. Das, *ACS Appl. Nano Mater.*, 2021, **4**, 10077–10089.
29 K. Dhara and R. M. Debiprosad, *Anal. Biochem.*, 2019, **586**, 113415.
30 Z. Ertekin and M. D. Symes, *Appl. Catal., A*, 2023, **666**, 119388.
31 L. Jiang, M. Gu, S. Zhao, H. Wang, X. Huang, A. Gao, H. Zhu, P. Sun, X. Liu, H. Lin and X. Zhang, *Small*, 2023, **19**, 1–10.
32 J. Zhang, T. Ha, M. Pham, Z. Gao, M. Li, Y. Ko, L. Lombardo and W. Zhao, *ACS Catal.*, 2023, **13**, 9326–9335.
33 L. Scarpetta-Pizo, R. Venegas, K. Muñoz-Becerra, L. Muñoz, A. Toro-Labbé, N. Darwish, R. Matute, R. Oñate, J. H. Zagal and I. Ponce, *Electrochim. Acta*, 2023, **468**, 143160.
34 X. Li, S. Surendran Rajasree, V. Gude, K. Maindan and P. Deria, *Angew. Chem., Int. Ed.*, 2023, **62**, e202219046.
35 X. Rozhkova, A. Aimukhanov, A. Zeinidenov, V. Paygin, D. Valiev, J. Bisquert, A. Guerrero, A. Alexeev and B. Ilyassov, *Synth. Met.*, 2023, **295**, 117347.

36 R. A. Shoukat Ali, J. Keshavayya, A. S. Jagadisha and S. D. Umesh, *Mater. Today: Proc.*, 2021, **36**, 853–856.
37 A. Kumar, V. Kumar Vashistha and D. Kumar Das, *Coord. Chem. Rev.*, 2021, **431**, 213678.
38 M. Chattanahalli Devendrachari, G. Shimoga, S. H. Lee, Y. H. Heo, H. Makri Nimbegondi Kotresh, R. R. Palem, S. Y. Kim and D. S. Choi, *ACS Appl. Energy Mater.*, 2023, **6**, 11199–11211.
39 N. M. Latiff, X. Fu, D. K. Mohamed, A. Veksha, M. Handayani and G. Lisak, *Carbon*, 2020, **168**, 245–253.
40 S. Gupta and M. De, *J. Electrochem. Soc.*, 2023, **170**, 46501.
41 H. Heli, M. Jafarian, M. G. Mahjani and F. Gobal, *Electrochimica Acta*, 2004, **49**, 4999–5006.
42 Y. Zhou, T. J. A. Slater, X. Luo and Y. Shen, *Appl. Catal., B*, 2023, **324**, 122218.
43 Z. Liu, M. Wu and J. Ma, *Phys. Chem. Chem. Phys.*, 2023, **25**, 7859–7868.
44 R. P. Putra, H. Horino and I. I. Rzeznicka, *Catalysts*, 2020, **10**, 233.
45 R. Georgescu, C. Boscornea, I. Calinescu and R. State, *Rev. Chim.*, 2015, **66**, 1554–1557.
46 D. S. Dalavi, P. N. Bhosale, C. A. Betty, A. K. Chauhan and P. S. Patil, *RSC Adv.*, 2012, **2**, 2100–2104.
47 A. Shaabani and Z. Hezarkhani, *Cellulose*, 2015, **22**, 3027–3046.
48 F.-D. Cong, B. Ning, X.-G. Du, C.-Y. Ma, H.-F. Yu and B. Chen, *Dyes Pigm.*, 2005, **66**, 149–154.
49 S. M. Sudhakara, M. C. Devendrachari, F. Khan, S. Thippeshappa and H. M. N. Kotresh, *Surf. Interfaces*, 2023, **36**, 102565.
50 R. Davis, A. N. Asokan and P. Predeep, *J. Inorg. Organomet. Polym. Mater.*, 2020, **30**, 4408–4415.
51 Y. Zhang and J. He, *J. Mater. Sci.*, 2022, **57**, 16064–16079.
52 K. B. Kokoh, F. Hahn, A. Métayer and C. Lamyl, *Electrochim. Acta*, 2002, **47**, 3965–3969.
53 D. N. Oko, S. Garbarino, J. Zhang, Z. Xu, M. Chaker, D. Ma, D. Guay and A. C. Tavares, *Electrochim. Acta*, 2015, **159**, 174–183.
54 Z.-J. Chen, J. Dong, J. Wu, Q. Shao, N. Luo, M. Xu, Y. Sun, Y. Tang, J. Peng and H.-M. Cheng, *Nat. Commun.*, 2023, **14**, 4210.
55 P. Mantos, C. Ferrone, T. Ohta, P. Choudhury and S. Chowdhury, *Appl. Surf. Sci.*, 2023, **614**, 156204.
56 C. Y. Chang, W. H. Huang, M. C. Tsai, C. W. Pao, J. L. Chen, M. Yoshimura, N. Hiraoka, C. L. Chen, B. J. Hwang and W. N. Su, *Mater. Today Nano*, 2024, **25**, 100466.
57 J. Mukherjee, S. Paul, A. Adalder, S. Kapse, R. Thapa, S. Mandal, B. Ghorai, S. Sarkar and U. K. Ghorai, *Adv. Funct. Mater.*, 2022, **32**, 1–9.
58 J. S. Stevens, S. J. Byard, C. C. Seaton, G. Sadiq, R. J. Davey and S. L. M. Schroeder, *Phys. Chem. Chem. Phys.*, 2014, **16**, 1150–1160.
59 T. Y. Qiu, Y. N. Zhao, W. S. Tang, H. Q. Tan, H. Y. Sun, Z. H. Kang, X. Zhao and Y. G. Li, *ACS Catal.*, 2022, **12**, 12398–12408.
60 X. An, Q. Tang, H. Lan, H. Liu, X. Yu, J. Qu, H. Lin and J. Ye, *Angew. Chem., Int. Ed.*, 2022, **134**, e2022127.
61 A. Arroquia, I. Acosta and M. P. G. Armada, *Mater. Sci. Eng., C*, 2020, **109**, 110602.
62 B. Pilarski, D. Wyrzykowski and J. Młodzianowski, *J. Solution Chem.*, 2023, **52**, 639–657.
63 B. G. Cox, *Acids and bases: solvent effects on acid-base strength*, OUP, Oxford, 2013.
64 A. E. Murekhina, D. N. Yarullin, M. A. Sovina, P. A. Kitaev and G. A. Gamov, *Inorganics*, 2022, **10**, 1–12.
65 A. Singh, A. Sharma, A. Ahmed and S. Arya, *Appl. Phys. A: Mater. Sci. Process.*, 2022, **128**, 1–12.
66 F. Khamespanah, M. Marx, D. B. Crochet, U. R. Pokharel, F. R. Fronczek, A. W. Maverick and M. Beller, *Nat. Commun.*, 2021, **12**, 10–13.
67 G. García-Díez, R. Monreal-Corona and N. Mora-Diez, *Antioxidants*, 2021, **10**, 1–20.
68 B. Zümreoglu-Karan, *Coord. Chem. Rev.*, 2006, **250**, 2295–2307.
69 D. D. Klyamer, A. S. Sukhikh, P. O. Krasnov, S. A. Gromilov, N. B. Morozova and T. V. Basova, *Appl. Surf. Sci.*, 2016, **372**, 79–86.
70 C. S. Martin, C. Gouveia-Caridade, F. N. Crespilho, C. J. L. Constantino and C. M. A. Brett, *J. Phys. Chem. C*, 2016, **120**, 15698–15706.
71 T. V. Basova, V. G. Kiselev, B. E. Schuster, H. Peisert and T. Chassé, *J. Raman Spectrosc.*, 2009, **40**, 2080–2087.
72 Y. Chen, M. Zhou, Y. Xia, X. Wang, Y. Liu, Y. Yao, H. Zhang, Y. Li, S. Lu, W. Qin, X. Wu and Q. Wang, *Joule*, 2019, **3**, 2255–2267.
73 Y. Jing, M. Wu, A. A. Wong, E. M. Fell, S. Jin, D. A. Pollack, E. F. Kerr, R. G. Gordon and M. J. Aziz, *Green Chem.*, 2020, **22**, 6084–6092.